




Cite this: *RSC Adv.*, 2025, 15, 42997

# Switchable supramolecular polymers of a Pt(II) complex *via* diacetylene $\pi$ -Ag<sup>+</sup> interaction

Yumi Park,<sup>a</sup> Woomin Jeong,<sup>b</sup> Ka Young Kim,<sup>c</sup> Jong-Man Kim <sup>b</sup>  
and Jong Hwa Jung <sup>\*ad</sup>

Controlling the driving forces during supramolecular polymerization represents a highly significant and challenging approach for the development of tailored supramolecular polymer systems for various applications. We report a switchable supramolecular polymerization system based on binuclear Pt(II) complex (Pt<sub>2</sub>L<sup>1</sup>) containing a diacetylene moiety, mediated by  $\pi$ -Ag<sup>+</sup> interactions between the diacetylene moieties and Ag<sup>+</sup> ions in a mixed DMSO/H<sub>2</sub>O (3:7 v/v) solvent system. The  $\pi$ -Ag<sup>+</sup> interaction functions as an additional driving force, significantly enhancing the strength of the supramolecular polymerization. Notably, the introduction of Ag<sup>+</sup> into the solution of Pt<sub>2</sub>L<sup>1</sup> led to a pronounced increase in photoluminescence intensity. The switchable behavior of the system was modulated through the sequential addition of a secondary ligand and metal ion. Thermodynamic parameters governing the supramolecular polymerization were elucidated by temperature-dependent photoluminescence spectroscopy.

Received 11th September 2025

Accepted 21st October 2025

DOI: 10.1039/d5ra06861d

rsc.li/rsc-advances

## Introduction

Building blocks containing diacetylene moieties are highly valuable components for the design of supramolecular polymers.<sup>1–5</sup> Diacetylene features a linear and rigid structure composed of two consecutive triple bonds, which imparts strong directionality and anisotropy.<sup>3,6–10</sup> This characteristic promotes the formation of well-defined one-dimensional supramolecular architectures such as fibers or ribbons.<sup>7,11–14</sup> Notably, diacetylene moieties exhibit photopolymerizable properties, enabling polymerization upon UV irradiation.<sup>8,9,15–17</sup> This photoreactivity makes them particularly attractive for the development of stimuli-responsive materials that exhibit color changes, fluorescence variation, or altered electrical properties.<sup>4,18,19</sup> However, photopolymerization of diacetylene requires precise molecular alignment, often referred to as topochemical conditions.<sup>15,17,20</sup> Specifically, the diacetylene units must be arranged at an optimal distance ( $\sim 4.9$  Å) and orientation ( $\sim 45^\circ$ ) relative to each other.<sup>9,15,16</sup> To achieve this, preorganization through non-covalent interactions such as  $\pi$ - $\pi$  stacking, hydrogen bonding, hydrophobic effects, or metal-ligand coordination is essential.<sup>13,17,18,20–25</sup> Therefore, when designing

diacetylene-containing building blocks, functional groups such as hydrogen bond donors/acceptors, aromatic rings, hydrophilic chains, or chiral centers are often introduced to guide the self-assembly and ensure appropriate alignment.<sup>4,5,13,26</sup>

More intriguingly, diacetylene moieties are capable of forming  $\pi$ -acetylene complexes with transition metal ions such as copper and silver.<sup>27–30</sup> In particular,  $\pi$ -complexation with Ag<sup>+</sup> can act as an additional driving force in supramolecular polymerization by promoting molecular alignment and stabilizing preorganized structures.<sup>29,31</sup> The physical properties and overall stability of diacetylene-based systems can also be finely tuned through strategic modification of substituents, while coordination with metal ions such as Ag<sup>+</sup> can facilitate both alignment and activation of reactive sites.<sup>30–35</sup> Supramolecular polymers derived from diacetylene-functionalized building blocks exhibit a range of advanced functionalities, including circularly polarized luminescence (CPL), Förster resonance energy transfer (FRET), and responsiveness to environmental stimuli.<sup>36–39</sup> These attributes make them highly attractive for use in next-generation functional materials, such as optical sensors, smart coatings, and bioresponsive systems.<sup>13,19,40–43</sup>

Although numerous supramolecular polymers incorporating diacetylene moieties have been reported over the past two decades,<sup>44–53</sup> no studies to date have explicitly demonstrated the  $\pi$ -interaction between diacetylene units and Ag<sup>+</sup> ions as a novel driving force in supramolecular polymerization. Therefore, elucidating and validating the role of diacetylene-Ag<sup>+</sup>  $\pi$ -complexation offers significant value and represents a promising advancement in the field of supramolecular polymer chemistry. Herein, we report a switchable supramolecular

<sup>a</sup>Department of Chemistry, Gyeongsang National University (GNU), Jinju 52828, Republic of Korea

<sup>b</sup>Department of Chemical Engineering, Hanyang University, Seoul 04763, Republic of Korea

<sup>c</sup>Technical Support Center for Chemical Industry, Korea Research Institute of Chemical Technology (KRICT), Ulsan 44429, Republic of Korea

<sup>d</sup>Research Institute of Advanced Chemistry, Gyeongsang National University (GNU), Jinju 52828, Republic of Korea. E-mail: jonghwa@gnu.ac.kr


polymerization system based on a Pt(II) complex (**Pt<sub>2</sub>L<sup>1</sup>**) containing a diacetylene moiety in the presence of Ag<sup>+</sup> ions in a mixed solvent of DMSO and H<sub>2</sub>O (3 : 7 v/v). Temperature-dependent photoluminescence (PL) changes of the supramolecular polymers, both in the presence and absence of Ag<sup>+</sup>, were systematically investigated to determine the Gibbs free energy and elucidate the underlying mechanism of supramolecular polymerization. Notably, the formation of a  $\pi$ -complex between **Pt<sub>2</sub>L<sup>1</sup>** and Ag<sup>+</sup> was confirmed through thermodynamic analysis and infrared spectroscopy. Furthermore, the reversibility of supramolecular polymer formation was demonstrated by introducing a secondary metal ion and ligand, highlighting the dynamic and switchable nature of the assembly process.

## Results and discussion

We synthesized a bis(terpyridine)-based platinum(II) complex incorporating diacetylene moieties (Fig. 1). Initially, compound **1** was obtained through a copper(I)-catalyzed oxidative homocoupling of propargyl alcohol in the presence of *N,N,N',N'*-tetramethylethylenediamine (TMEDA) and molecular oxygen in acetonitrile, followed by oxidation with Jones reagent to yield the corresponding dicarboxylic acid. In parallel, a terpyridine-based amine intermediate was prepared by nucleophilic substitution of 4'-chloro-2,2':6',2''-terpyridine with 3-amino-1-propanol in DMSO under basic conditions. This intermediate was subsequently coupled with compound **1** via EDC·HCl-mediated amidation in the presence of HOBt and NaHCO<sub>3</sub> in DMF, affording the diacetylene-bridged bis(terpyridine) ligand **L<sup>1</sup>**. The final platinum(II) complex, **Pt<sub>2</sub>L<sup>1</sup>**, was synthesized by coordinating **Pt<sub>2</sub>L<sup>1</sup>** with cyclooctadiene platinum(II) dichloride in methanol. The structure and purity of the resulting complex were confirmed by spectroscopic techniques, including NMR and mass spectrometry.

The formation of supramolecular polymers (SPs) was evaluated in various solvents, including pure DMSO, methanol, THF, and acetonitrile. **Pt<sub>2</sub>L<sup>1</sup>** (100  $\mu$ M) was readily soluble only in DMSO, but was insoluble in methanol, THF, and acetonitrile. Accordingly, UV-vis absorption and photoluminescence (PL) spectra of **Pt<sub>2</sub>L<sup>1</sup>** were recorded in mixed DMSO/H<sub>2</sub>O at varying volume ratios to investigate its supramolecular polymerization.

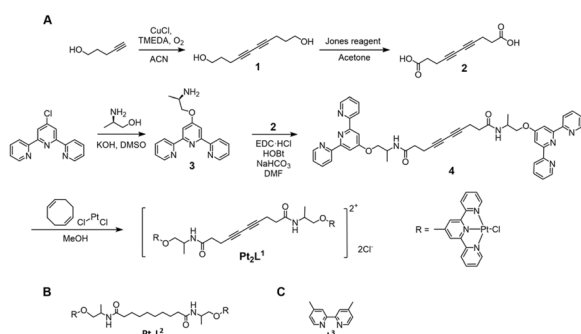


Fig. 1 (A) Synthetic procedures for **Pt<sub>2</sub>L<sup>1</sup>**. (B and C) Chemical structures of **Pt<sub>2</sub>L<sup>2</sup>** and **L<sup>3</sup>** used in this study.

With increasing water content, the intense high-energy absorption band in the 250–320 nm region—attributed to intraligand [ $\pi \rightarrow \pi^*$ ] transitions within the terpyridine moieties—decreased a marked decrease (Fig. 2A and C), consistent with enhanced  $\pi$ - $\pi$  stacking between terpyridine units during supramolecular polymerization.<sup>54–57</sup>

In contrast, the absorption bands observed between 350 and 490 nm, corresponding to a metal-to-ligand charge transfer (MLCT) transition [ $d\pi(\text{Pt}) \rightarrow \pi^*(\text{terpyridine})$ ], as well as a ligand-to-ligand charge transfer (LLCT) [ $\pi(\text{terpyridine}) \rightarrow \pi^*(\text{terpyridine})$ ] contribution, exhibited only minor changes. Notably, the PL intensity of **Pt<sub>2</sub>L<sup>1</sup>** (100  $\mu$ M) increased significantly around 564 nm in DMSO/H<sub>2</sub>O mixtures of 3 : 7 and 1 : 9 (v/v) (Fig. 2B and C), consistent with MLCT emission. These results strongly suggest that **Pt<sub>2</sub>L<sup>1</sup>** undergoes supramolecular polymerization in aqueous-rich DMSO mixtures, particularly at 3 : 7 and 1 : 9 DMSO/H<sub>2</sub>O ratios.

Based on these results, the optimal condition for supramolecular polymerization was identified as a 3 : 7 (v/v) mixture of DMSO and H<sub>2</sub>O.

To gain insight into the morphology of the SP derived from **Pt<sub>2</sub>L<sup>1</sup>**, atomic force microscopy (AFM) was employed in a mixed DMSO and H<sub>2</sub>O (3 : 7 v/v). As shown in Fig. 3, the AFM image reveals a network of fibrillar structures with heights ranging from 1 to 2 nm (Fig. S1), along with partially two-dimensional (2D) sheet-like architectures (Fig. 3B) formed through the well-ordered arrangement of fibrils. Furthermore, the quantum yield (QY) and fluorescence lifetime ( $\tau$ ) of the SPs in a mixed DMSO and H<sub>2</sub>O (3 : 7 v/v) were determined to be 0.024 and 8.0 ns, respectively (Fig. S2). Therefore, the enhanced PL intensity of **Pt<sub>2</sub>L<sup>1</sup>** at approximately 564 nm in a mixed DMSO and H<sub>2</sub>O (3 : 7 v/v) further supports the occurrence of supramolecular polymerization, corresponding to MLCT.

To elucidate the role of intermolecular hydrogen bonding in the assembly of SPs, Fourier transform infrared (FT-IR) spectroscopy was employed. The amide I band (C=O) of the SP based on **Pt<sub>2</sub>L<sup>1</sup>** prepared in mixed DMSO/H<sub>2</sub>O (3 : 7 v/v) appears

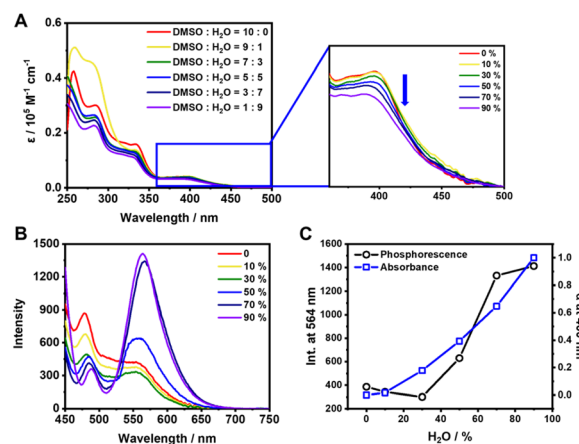


Fig. 2 (A) UV and (B) PL spectra of **Pt<sub>2</sub>L<sup>1</sup>** at the varying solvent ratio (DMSO/H<sub>2</sub>O) (C) Plot of PL intensity and absorbance vs. content of H<sub>2</sub>O.



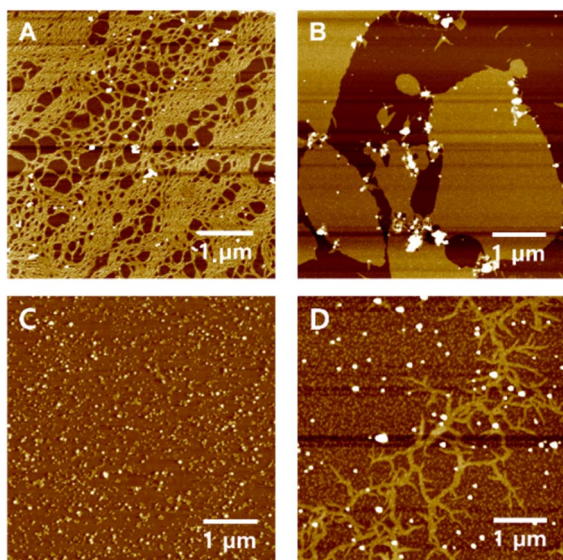


Fig. 3 AFM Images of  $\text{Pt}_2\text{L}^1$  (100  $\mu\text{M}$ ) in the (A and B) absence and (C) presence of  $\text{AgNO}_3$  (2 equiv.) and (D) upon addition of  $\text{L}^3$  (10 equiv.) in a mixed DMSO and  $\text{H}_2\text{O}$  (3 : 7 v/v).

at  $1666\text{ cm}^{-1}$  (Fig. S3), whereas that of the SP prepared in pure DMSO appears at  $1740\text{ cm}^{-1}$ . This pronounced red shift indicates that  $\text{Pt}_2\text{L}^1$  forms supramolecular polymers through intermolecular hydrogen-bonding interactions ( $\text{C}=\text{O}\cdots\text{H}-\text{N}$ ) between amide groups. Supplementing these observations,  $^1\text{H}$  NMR studies performed in  $\text{DMSO}-d_6/\text{D}_2\text{O}$  (3 : 7 v/v) at 298 K showed broadening of the aromatic proton peaks for  $\text{Pt}_2\text{L}^1$  (Fig. S4), a feature attributed to the assembly of these molecules into supramolecular polymers. At elevated temperature (363 K), these aromatic proton peaks displayed more pronounced low-field shifts and improved resolution, signifying the disassembly into monomeric species. Taken together, these FT-IR and  $^1\text{H}$  NMR spectral data strongly support the notion that intermolecular hydrogen bonding, along with  $\pi$ - $\pi$  stacking interactions, serve as the principal driving forces underlying the formation of these SPs. Also, three peaks for self-assembled  $\text{Pt}_2\text{L}^1$  were observed at  $q = 4.64$ ,  $8.89$ , and  $19.5\text{ nm}^{-1}$  by XRD observation (Fig. S5A), corresponding to real-space spacings of  $d = 1.35$ ,  $0.71$ , and  $0.34\text{ nm}$ , respectively. The  $1.35\text{ nm}$  spacing is smaller than the fully extended molecular length ( $3.31\text{ nm}$ ) of  $\text{Pt}_2\text{L}^1$ , indicating that the self-assembled  $\text{Pt}_2\text{L}^1$  forms a monolayer structure with a slightly tilted molecular orientation. Based on UV-vis, FT-IR,  $^1\text{H}$  NMR and XRD analyses, the proposed packing model for the  $\text{Pt}_2\text{L}^1$ -based SP is shown in Fig. S6. The molecular length is approximately  $3.31\text{ nm}$  according to DFT calculations.

The SP adopts a monolayer structure stabilized by intermolecular hydrogen bonding between amide groups and  $\pi$ - $\pi$  stacking interactions.

To determine the thermodynamic parameters, temperature-dependent PL spectral changes were examined in a mixed DMSO and  $\text{H}_2\text{O}$  (3 : 7 v/v) solution. With increasing temperature, the PL intensity corresponding to the MLCT band at approximately  $564\text{ nm}$  decreased (Fig. 4), whereas it gradually

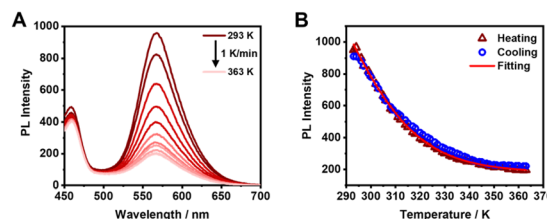


Fig. 4 Temperature-dependent PL spectra (A) PL Spectra of  $\text{Pt}_2\text{L}^1$  (50  $\mu\text{M}$ ) in  $\text{DMSO}/\text{H}_2\text{O}$  (3 : 7 v/v) about heating data. (B) Plots of PL Intensity at  $564\text{ nm}$ .

increased with decreasing temperature. These PL spectral changes are attributed to the reversible transition between SP formation and monomer dissociation. The heating and cooling profiles of  $\text{Pt}_2\text{L}^1$  (50  $\mu\text{M}$ ) exhibited sigmoidal behavior with no observable hysteresis between the two curves (Fig. 4), indicating a rapid and reversible disassembly into monomers. These results suggest that the supramolecular polymerization follows an isodesmic mechanism. Therefore, the thermodynamic parameters were determined by curve fitting based on the isodesmic model using MatLab. The Gibbs free energy ( $\Delta G$ ), enthalpy ( $\Delta H$ ), and binding constant ( $K$ ) were calculated to be  $-25.5\text{ kJ mol}^{-1}$ ,  $-65.7\text{ kJ mol}^{-1}$ , and  $3.55 \times 10^4$ , respectively (Table S1). In addition, the cooperativity value ( $\sigma = K_n/K_e$ ) is approximately 1, further confirming that the SPs follow an isodesmic model.

To reinforce supramolecular polymerization through the formation of  $\pi$ - $\text{Ag}^+$  interactions in  $\text{Pt}_2\text{L}^1$ , various concentrations of  $\text{Ag}^+$  ions were added to a  $\text{Pt}_2\text{L}^1$  solution (100  $\mu\text{M}$ ) in a mixed  $\text{DMSO}/\text{H}_2\text{O}$  (3 : 7 v/v) solvent system. As shown in Fig. 5, the PL intensity of  $\text{Pt}_2\text{L}^1$  exhibited a slight increase with  $\text{Ag}^+$  concentrations below 1.0 equivalent, and no precipitation was observed (Fig. S7), despite the presence of  $\text{Cl}^-$  anions.

Notably, when the  $\text{Ag}^+$  concentration exceeded 1.0 equivalent, the PL intensity sharply increased up to 2.0 equivalents, indicating the formation of  $\pi$ - $\text{Ag}^+$  interactions involving the diacetylene moieties. Therefore, at 1.0 equiv. of  $\text{Ag}^+$ , a single  $\text{C}\equiv\text{C}$  site is preferentially engaged in a monocoordination bond. In contrast, at 2.0 equiv.,  $\text{Ag}^+$  coordinates to both  $\text{C}\equiv\text{C}$  sites, acting as a bridging node that links neighbouring ligands and triggers supramolecular polymerization. The quantum yield (QY) and fluorescence lifetime ( $\tau$ ) of the SPs in the presence of  $\text{Ag}^+$  (2.0 equiv.) were also determined to be 0.022 and 9.5

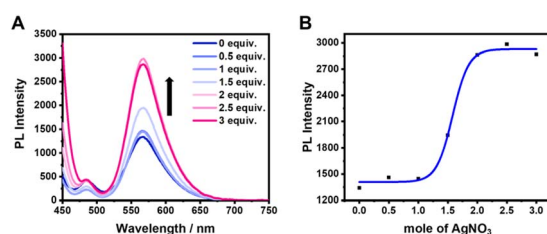


Fig. 5 (A) PL spectral changes of  $\text{Pt}_2\text{L}^1$  by addition of  $\text{AgNO}_3$  from 0 equiv. to 3 equiv. in  $\text{DMSO}$  and  $\text{H}_2\text{O}$  (3 : 7 v/v). (B) Plot of PL Intensity at  $564\text{ nm}$ .





ns, respectively, in a mixed DMSO and H<sub>2</sub>O (3 : 7 v/v) solution (Fig. S8).

To confirm the formation of  $\pi$ -Ag<sup>+</sup> interactions involving the diacetylene moiety, FT-IR spectroscopy was employed to monitor the vibrational changes of the diacetylene group in **Pt<sub>2</sub>L<sup>1</sup>** upon the addition of Ag<sup>+</sup> (2.0 equiv.). In the absence of Ag<sup>+</sup>, the C≡C stretching band of the diacetylene group appeared at approximately 2071 cm<sup>-1</sup> (Fig. S9). However, upon addition of Ag<sup>+</sup>, this band disappeared, suggesting that the vibrational mode became IR-inactive due to the formation of a  $\pi$ -Ag<sup>+</sup> complex. This spectral behavior is consistent with previously reported studies involving  $\pi$ -metal interactions.<sup>27,58–60</sup> Upon heating, the aromatic protons shifted downfield (Fig. S10A). Interestingly, the sharp single peak (2.18 ppm) of proton H9 at 293 K split into two distinct peaks at 333 K (Fig. S10B). Thus, the peak of H9 at 293 K corresponds to the supramolecular polymer with Ag<sup>+</sup> ions, whereas the new peak at 2.21 ppm is assigned to the monomeric **Pt<sub>2</sub>L<sup>1</sup>** species generated by disassembly. These findings suggest that Ag<sup>+</sup> ions are coordinated to the acetylene moiety of **Pt<sub>2</sub>L<sup>1</sup>**. Also, upon addition of Ag<sup>+</sup>, a new peak appeared at  $q = 19.5 \text{ nm}^{-1}$  ( $d \approx 3.2 \text{ \AA}$ ) by XRD observation (Fig. S5B), which likely corresponds to  $\pi$ -Ag<sup>+</sup> interactions. Furthermore, the AFM image of the SPs in the presence of Ag<sup>+</sup> (2.0 equiv.) reveals spherical nanostructures with heights ranging from 15 to 30 nm (Fig. 2C and S11). To remove Ag<sup>+</sup> bound to the acetylene moieties, Cl<sup>-</sup> or **L<sup>3</sup>** (5 equiv.) was added to the spherical solution. As a result, the PL intensity was restored to that of the original **Pt<sub>2</sub>L<sup>1</sup>** solution (Fig. 6 and S12). Furthermore, the spherical nanostructures transformed into fibrous structures upon the addition of Cl<sup>-</sup> or **L<sup>3</sup>** as a secondary ligand (Fig. 2D), both of which exhibit high affinity for Ag<sup>+</sup>, indicating that the supramolecular polymerization could be modulated by Ag<sup>+</sup> or **L<sup>3</sup>**.

In the presence of AgNO<sub>3</sub> (2.0 equiv.),  $\Delta G$  and  $\Delta H$  of the SP were  $-27.5 \text{ kJ mol}^{-1}$  and  $-106.8 \text{ kJ mol}^{-1}$ , respectively (Fig. S13 and Table S1). The  $\sigma$  value was calculated to be approximately 1, confirming that the SP formed in the presence of Ag<sup>+</sup> follow an isodesmic polymerization model. These results indicate that the introduction of Ag<sup>+</sup> significantly enhances the stability of the SP. As a control experiment, the PL intensity of the self-assembled **Pt<sub>2</sub>L<sup>2</sup>** complex, which lacks a diacetylene moiety, was monitored upon the addition of Ag<sup>+</sup> (1.0 and 2.0 equiv.) in a mixed DMSO and H<sub>2</sub>O (3 : 7 v/v) solvent system. Notably, no significant changes in PL intensity were observed (Fig. S14),

further supporting the conclusion that Ag<sup>+</sup> ions specifically interact with the diacetylene moiety of **Pt<sub>2</sub>L<sup>1</sup>** through  $\pi$ -Ag<sup>+</sup> coordination.

To reversibly modulate the PL intensity during supramolecular polymerization as shown in Fig. 6, a secondary ligand (**L<sup>3</sup>**, 5.0 equiv.) was introduced into the SP solution containing Ag<sup>+</sup> (2.0 equiv.) (Fig. 6). This addition was intended to sequester Ag<sup>+</sup> ions coordinated to the diacetylene moiety of **Pt<sub>2</sub>L<sup>1</sup>**. Consequently, the PL intensity at approximately 564 nm and the morphology reverted to the level observed in the absence of Ag<sup>+</sup>, indicating that **L<sup>3</sup>** effectively captured Ag<sup>+</sup> through a ligand exchange process. Subsequently, Zn<sup>2+</sup> ions were added to the solution to induce re-coordination of Ag<sup>+</sup> to **Pt<sub>2</sub>L<sup>1</sup>** by displacing it from the **L<sup>3</sup>**-Ag<sup>+</sup> complex (Fig. S15). As anticipated, the PL intensity increased to the same level observed in the initial **Pt<sub>2</sub>L<sup>1</sup>**/Ag<sup>+</sup> system (Fig. S15), consistent with the formation of a stronger Zn<sup>2+</sup>-**L<sup>3</sup>** complex compared to the **L<sup>3</sup>**-Ag<sup>+</sup> complex, thereby liberating Ag<sup>+</sup> to rebind with **Pt<sub>2</sub>L<sup>1</sup>**. Finally, tetramethylammonium chloride (20 equiv.) was introduced to the **Pt<sub>2</sub>L<sup>1</sup>**-Ag<sup>+</sup> solution to effectively sequester Ag<sup>+</sup> ions. Upon this addition, the PL intensity returned to nearly the same level as that of the original SP solution without Ag<sup>+</sup> (Fig. S16), confirming the complete removal of Ag<sup>+</sup>. These findings demonstrate that the PL intensity of the supramolecular architectures can be reversibly modulated through the strategic introduction of secondary metal ions and ligands, enabling a switchable optical response (Fig. 6B).

## Conclusions

We have developed a switchable supramolecular polymerization system based on a binuclear Pt(II) complex (**Pt<sub>2</sub>L<sup>1</sup>**) bearing diacetylene moieties, wherein  $\pi$ -Ag<sup>+</sup> interactions between the diacetylene units and Ag<sup>+</sup> ions serve as an auxiliary driving force in a mixed DMSO/H<sub>2</sub>O (3 : 7 v/v) solvent system. These  $\pi$ -Ag<sup>+</sup> interactions not only promote supramolecular polymerization but also represent a novel strategy for enhancing polymerization efficiency through metal- $\pi$  coordination. The resulting supramolecular polymer of **Pt<sub>2</sub>L<sup>1</sup>** assembles *via* an isodesmic mechanism. Furthermore, the polymerization process can be reversibly modulated by the addition of a secondary ligand and/or metal ion, demonstrating a switchable behavior. Thermodynamically, the Gibbs free energy for the polymer formed in the presence of Ag<sup>+</sup> is slightly higher than that without Ag<sup>+</sup>, suggesting a subtle stabilization effect. Notably, the introduction of Ag<sup>+</sup> also induces a significant enhancement in the photoluminescence intensity, highlighting the dual functional role of Ag<sup>+</sup> in both structural and optical modulation of the supramolecular polymer. Thus, we anticipate that this approach will serve as a versatile and robust framework for developing switchable supramolecular polymers, opening new avenues for applications in materials chemistry and beyond.

## Conflicts of interest

There are no conflicts to declare.

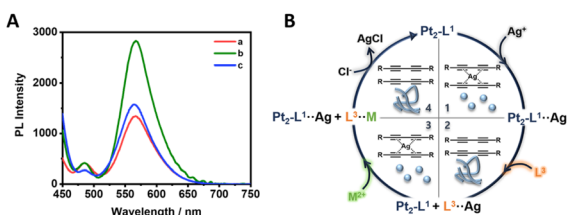


Fig. 6 (A) PL spectral changes of **Pt<sub>2</sub>L<sup>1</sup>** (100  $\mu$ M) in the (a) absence and (b) presence of AgNO<sub>3</sub> (2.0 equiv.) and (c) upon addition of **L<sup>3</sup>** (5.0 equiv.) in DMSO/H<sub>2</sub>O (v/v = 3 : 7). (B) The circular diagram of switchable  $\pi$ -Ag<sup>+</sup> interaction.



## Data availability

Additional experimental details as well as the data supporting this article, including materials and methods,  $^1\text{H}$  NMR,  $^{13}\text{C}$  NMR, and FT-IR spectra and thermodynamic parameters, have been included as part of the supplementary information (SI). Supplementary information: additional experimental procedures, NMR spectra, and supporting figures. See DOI: <https://doi.org/10.1039/d5ra06861d>.

## Acknowledgements

This research was supported by a National Foundation of Korea (NRF) grant funded by the Korean Government (MSIT) (grants 2021R1A2C2007664 and RS-2025-02214848) and the Korea Research Institute of Chemical Technology (project number KS2541-20 and BSK25-139). This work was supported by the Gyeongsang National University Fund for Professors on Sabbatical Leave, 2023.

## Notes and references

- 1 N. Bäumer, J. Matern and G. Fernández, *Chem. Sci.*, 2021, **12**, 12248–12265.
- 2 B. Yoon, S. Lee and J.-M. Kim, *Chem. Soc. Rev.*, 2009, **38**, 1958–1968.
- 3 E. Jahnke, I. Lieberwirth, N. Severin, J. P. Rabe and H. Frauenrath, *Angew. Chem., Int. Ed.*, 2006, **45**, 5383–5386.
- 4 O. Yarimaga, J. Jaworski, B. Yoon and J.-M. Kim, *Chem. Commun.*, 2012, **48**, 2469–2485.
- 5 E. Jahnke, J. Weiss, S. Neuhaus, T. N. Hoheisel and H. Frauenrath, *Chem.–Eur. J.*, 2008, **15**, 388–404.
- 6 L. Juhasz, R. D. Ortuso and K. Sugihara, *Nano Lett.*, 2021, **21**, 543–549.
- 7 L. Hsu, G. L. Cvetanovich and S. I. Stupp, *J. Am. Chem. Soc.*, 2008, **130**, 3892–3899.
- 8 A. Dhaka, I. R. Jeon, O. Jeannin, E. Aubert, E. Espinosa and M. Fourmigué, *Angew. Chem., Int. Ed.*, 2022, **61**, e202116650.
- 9 D.-Y. Kim, S.-A. Lee, D. Jung, J. Koo, J. S. Kim, Y.-T. Yu, C.-R. Lee and K.-U. Jeong, *Soft Matter*, 2017, **13**, 5759–5766.
- 10 R. Jelinek and M. Ritenberg, *RSC Adv.*, 2013, **3**, 21192–21201.
- 11 J. P. Hill, W. Jin, A. Kosaka, T. Fukushima, H. Ichihara, T. Shimomura, K. Ito, T. Hashizume, N. Ishii and T. Aida, *Science*, 2004, **304**, 1481–1483.
- 12 T. Shimizu, M. Masuda and H. Minamikawa, *Chem. Rev.*, 2005, **105**, 1401–1443.
- 13 G. P. Maurya, D. Verma, A. Sinha, L. Brunsveld and V. Haridas, *Angew. Chem., Int. Ed.*, 2022, **61**, e202209806.
- 14 H. Jiang, X. Y. Hu, S. Schlesiger, M. Li, E. Zellermann, S. K. Knauer and C. Schmuck, *Angew. Chem., Int. Ed.*, 2017, **56**, 14526–14530.
- 15 K. Hema, A. Ravi, C. Raju, J. R. Pathan, R. Rai and K. M. Sureshan, *Chem. Soc. Rev.*, 2021, **50**, 4062–4099.
- 16 K. Hema, A. Ravi, C. Raju and K. M. Sureshan, *Chem. Sci.*, 2021, **12**, 5361–5380.
- 17 J. Fan, X. Xu, W. Yu, Z. Wei and D. Zhang, *Polym. Chem.*, 2020, **11**, 1947–1953.
- 18 K. Bae, D. G. Lee, M. I. Khazi and J.-M. Kim, *Macromolecules*, 2022, **55**, 2882–2891.
- 19 X. Qian and B. Städler, *Chem. Mater.*, 2019, **31**, 1196–1222.
- 20 Y. Li, K. M.-C. Wong, H.-L. Wong and V. W.-W. Yam, *ACS Appl. Mater. Interfaces*, 2016, **8**, 17445–17453.
- 21 P. A. Korevaar, S. J. George, A. J. Markvoort, M. M. J. Smulders, P. A. J. Hilbers, A. P. H. J. Schenning, T. F. A. De Greef and E. W. Meijer, *Nature*, 2012, **481**, 492–495.
- 22 J. Matern, Z. Fernández, N. Bäumer and G. Fernández, *Angew. Chem., Int. Ed.*, 2022, **61**, e202203783.
- 23 X. Yu, Z. Wang, Y. Li, L. Geng, J. Ren and G. Feng, *Inorg. Chem.*, 2017, **56**, 7512–7518.
- 24 M. F. J. Mabesoone, A. R. A. Palmans and E. W. Meijer, *J. Am. Chem. Soc.*, 2020, **142**, 19781–19798.
- 25 B. Hosseinzadeh and M. Ahmadi, *Coord. Chem. Rev.*, 2022, **471**, 214733.
- 26 E. Krieg, M. M. C. Bastings, P. Besenius and B. Rybtchinski, *Chem. Rev.*, 2016, **116**, 2414–2477.
- 27 F. Rey-Tarrio, S. Simón-Fuente, J. M. Cuerva, D. Miguel, M. Ribagorda, E. Quiñoá and F. Freire, *Angew. Chem., Int. Ed.*, 2024, **63**, e202318454.
- 28 G. Fang and X. Bi, *Chem. Soc. Rev.*, 2015, **44**, 8124–8173.
- 29 Y. Zhu, W. Zheng, W. Wang and H.-B. Yang, *Chem. Soc. Rev.*, 2021, **50**, 7395–7417.
- 30 P. Sivaguru, S. Cao, K. R. Babu and X. Bi, *Acc. Chem. Res.*, 2020, **53**, 662–675.
- 31 S. Yang, T. Zhou, X. Yu and M. Szostak, *Molecules*, 2023, **28**, 950.
- 32 C. Li, M. Ok, H. Choi and J. H. Jung, *New J. Chem.*, 2022, **46**, 3551–3554.
- 33 H. Schmidbaur and A. Schier, *Angew. Chem., Int. Ed.*, 2015, **54**, 746–784.
- 34 D.-D. Tao, J.-H. Wei, X.-S. Yan, Q. Wang, B.-H. Kou, N. Chen and Y.-B. Jiang, *Chem. Commun.*, 2020, **56**, 15133–15136.
- 35 R. M. Rawashdeh-Omary, M. A. Omary and H. H. Patterson, *J. Am. Chem. Soc.*, 2000, **122**, 10371–10380.
- 36 C. He, G. Yang, Y. Kuai, S. Shan, L. Yang, J. Hu, D. Zhang, Q. Zhang and G. Zou, *Nat. Commun.*, 2018, **9**, 5117.
- 37 J. Seo, M. I. Khazi, K. Bae and J.-M. Kim, *Small*, 2023, **19**, 2206428.
- 38 D. Zhai, J. Jiang, C. Yuan, D. Wang, Y. Jiang and M. Liu, *Adv. Optical Mater.*, 2023, **11**, 2300161.
- 39 A. J. P. Teunissen, C. Pérez-Medina, A. Meijerink and W. J. M. Mulder, *Chem. Soc. Rev.*, 2018, **47**, 7027–7044.
- 40 F. Fang, F. Meng and L. Luo, *Mater. Chem. Front.*, 2020, **4**, 1089–1104.
- 41 X. Qian and B. Städler, *Adv. Funct. Mater.*, 2020, **30**, 2004605.
- 42 Z.-B. Jin, G. Zhou, Y. Han, Z. Huang, Z.-G. Gu and J. Zhang, *J. Am. Chem. Soc.*, 2024, **146**, 25016–25027.
- 43 S. Shanmugaraju, H. Jadhav, R. Karthik and P. S. Mukherjee, *RSC Adv.*, 2013, **3**, 4940–4950.
- 44 Z. Li, F. W. Fowler and J. W. Lauher, *J. Am. Chem. Soc.*, 2009, **131**, 634–643.
- 45 J.-M. Heo, Y. Son, S. Han, H.-J. Ro, S. Jun, U. Kundapur, J. Noh and J.-M. Kim, *Macromolecules*, 2019, **52**, 4405–4411.

- 46 G. Shin, M. I. Khazi and J.-M. Kim, *Macromolecules*, 2020, **53**, 149–157.
- 47 D. Jang, J.-M. Heo, F. Jannah, M. I. Khazi, Y. J. Son, J. Noh, H. An, S. M. Park, D. K. Yoon, N. N. Kadamannil, R. Jelinek and J.-M. Kim, *Angew. Chem., Int. Ed.*, 2022, **61**, e202211465.
- 48 S. Li, L. Zhang, J. Jiang, Y. Meng and M. Liu, *ACS Appl. Mater. Interfaces*, 2017, **9**, 37386–37394.
- 49 X. Wang, X. Sun, P. A. Hu, J. Zhang, L. Wang, W. Feng, S. Lei, B. Yang and W. Cao, *Adv. Funct. Mater.*, 2013, **23**, 6044–6050.
- 50 M. van den Heuvel, D. W. P. M. Löwik and J. C. M. van Hest, *Biomacromolecules*, 2008, **9**, 2727–2734.
- 51 L. Zhu, M. T. Trinh, L. Yin and Z. Zhang, *Chem. Sci.*, 2016, **7**, 2058–2065.
- 52 Q. Li, S. Ren, Y. Peng, Y. Lv, W. Wang, Z. Wang and Z. Gao, *Anal. Chem.*, 2020, **92**, 1611–1617.
- 53 N. Lv, T. Ma, H. Qin, Z.-R. Yang, Y. Wu, D. Li, J. Tao, H. Jiang and J. Zhu, *Sci. China-Mater.*, 2022, **65**, 2861–2870.
- 54 S. Lim, Y. Cho, J. H. Kang, M. Hwang, Y. Park, S. K. Kwak, S. H. Jung and J. H. Jung, *J. Am. Chem. Soc.*, 2024, **146**, 18484–18497.
- 55 M. Kim, M. Ok, C. Li, K. Go, S. Kim, J. Kim, J. H. Jung and S. H. Jung, *Inorg. Chem. Front.*, 2023, **10**, 768–775.
- 56 M. Ok, K. Y. Kim, H. Choi, S. Kim, S. S. Lee, J. Cho, S. H. Jung and J. H. Jung, *Chem. Sci.*, 2022, **13**, 3109–3117.
- 57 M. Kim, H. Choi, M. Kim, S. Kim, S. Yun, E. Lee, J. Cho, S. H. Jung and J. H. Jung, *Chem. Sci.*, 2024, **15**, 19729–19738.
- 58 A. Noonikara-Poyil, S. G. Ridlen, I. Fernández and H. V. R. Dias, *Chem. Sci.*, 2022, **13**, 7190–7203.
- 59 E. Nagy, E. J. StGermain, P. Cosme, P. Maity, A. C. Terentis and S. D. Lepore, *Chem. Commun.*, 2016, **52**, 2311–2313.
- 60 A. S. Mahadevi and G. N. Sastry, *Chem. Rev.*, 2013, **113**, 2100–2138.

